Sensors and Materials, Vol. 35, No. 9 (2023) 3189–3200
MYU Tokyo

S & M 3384

Development of a Humidity Microsensor for Evaluation of Hermeticity for Retinal Prosthesis

Takuro Kono,[1,2*] Yasuo Terasawa,[1,3] Hiroyuki Tashiro,[2,4] and Jun Ohta[2,3]

[1]Artificial Vision Institute, R and D Div., Nidek Co., Ltd., 13-2 Hama-cho, Gamagori, Aichi 443-0036, Japan
[2]Division of Materials Science, Nara Institute of Science and Technology,
8916-5 Takayama-cho, Ikoma, Nara 630-0192, Japan
[3]Institute for Research Initiatives, Nara Institute of Science and Technology,
8916-5 Takaya-cho, Ikoma, Nara 630-0192, Japan
[4]Division of Medical Technology, Department of Health Sciences, Faculty of Medical Sciences, Kyushu University,
3-1-1 Maidashi, Higashi-ku, Fukuoka 812-8582, Japan

(Received April 28, 2023; accepted August 24, 2023)

Keywords: humidity microsensor, microhermetic package, long-term reliability, retinal prosthesis, accelerated life testing

Retinal prosthesis requires a microhermetic package with long-term reliability for the intraocular implantation of devices. The evaluation of the hermetic package generally involves leak testing, but it is challenging to detect micropackages by leak tests owing to their small volume. Therefore, a sensor that can sense the environment inside the package is necessary. However, conventional sensors are too large to be mounted inside a micropackage. To address this issue, we fabricated a humidity microsensor that is compatible with a microhermetic package and evaluated its performance. The humidity microsensor was fabricated by layering a sensitive film on glass using a simple photolithography technique. The humidity microsensor exhibited a linear response to changes in relative humidity in a 25 ℃ environment with a capacitance change of 0.059 pF. By using the humidity microsensor, we successfully detected device failure in the microhermetic package. Moreover, the fabricated humidity microsensor operated stably for >14 days under transient thermal stress at 200 ℃ during hermetic sealing and under continuous thermal stress during accelerated testing at 87 ℃. These results demonstrate that the fabricated humidity microsensor is useful for evaluating the long-term reliability of microhermetic packages.

1. Introduction

Retinal prosthesis is a general term for devices that provide visual information to the retina to replace lost light perception. Our group has developed a device based on the suprachoroidal-transretinal stimulation method and demonstrated its effectiveness.(1) Improving the performance of retinal prosthesis devices requires a high resolution and a wide field of view, which necessitates an increase in the number of electrodes and a stimulatable area. However, increasing

*Corresponding author: e-mail: takurou_kouno@nidek.co.jp
https://doi.org/10.18494/SAM4476

ISSN 0914-4935
https://myukk.org/

the number of electrodes leads to a larger IC size that controls the stimulation current, and manufacturing difficulty increases with additional wiring. To solve these problems, we suggest a method of controlling multiple electrodes using a small IC and modularizing of the system.[2] The retinal prosthesis under consideration is a chip-mounted device with eight modules connected by a small number of wires, which is capable of stimulating >150 electrodes (Fig. 1). To produce this device, a packaging technology with a size below 1 mm^2 that is reliable over a long term should be established. For instance, the long-term reliability of retinal prosthesis devices requires a lifespan of more than five years *in vivo*.[3] The hermetic package that protects the electronics from the biological environment plays a crucial role in ensuring the long-term reliability of implantable devices. MIL-STD-883[4] outlines the reliability evaluation methods for hermetic packages, where the gross leakage and He leakage tests are the principal tests for industrial evaluation, based on the package size and leakage rate. However, measuring the leakage rate required for implantable devices necessitates expensive equipment to detect ultrafine leaks. Moreover, as the He leakage test, which detects fine leaks, pressurizes the package, the package must be strong enough to withstand pressurization. Additionally, conventional package materials such as glass are permeable to He,[5] making it difficult to determine whether leakage is from inside the package or has diffused into the glass at the required leak rate for the device. Consequently, there are restrictions on the encapsulating material composition that can be used for the test. Apart from the He leakage test, tests using the Ca conductance[6] and Cu corrosion as indicators[7] have been performed to assess moisture penetration in the package. However, these methods are limited to specific atmospheric conditions and hermetic sealing temperatures and have a low detection speed. Therefore, an effective method that has a high detection speed and can be applied to general hermetic encapsulation processes is to mount a humidity sensor inside a package and evaluate it.[8]

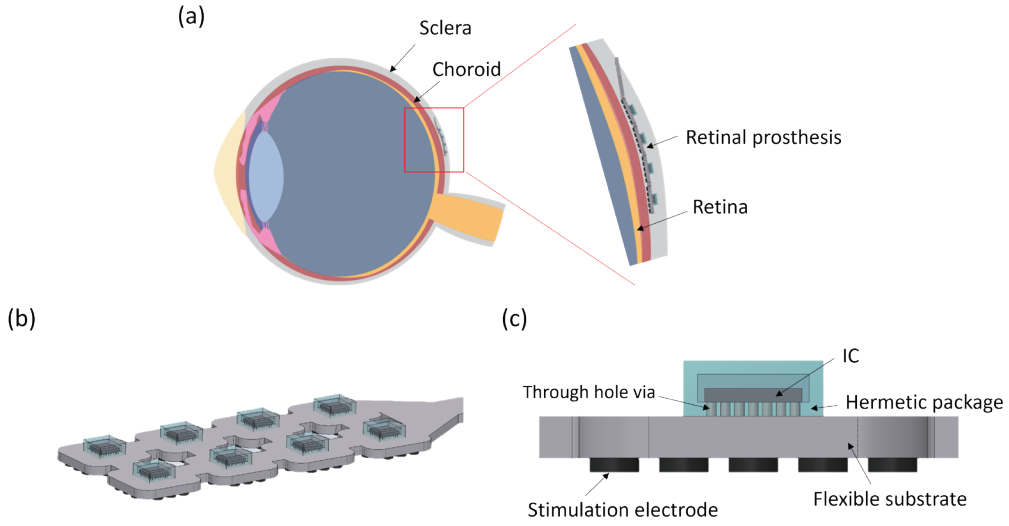

Fig. 1. (Color online) (a) Schematic of retinal prosthesis in eye. (b) Top view of retinal prosthesis. (c) Side view of retinal prosthesis.

Humidity sensors can be roughly classified into two types: resistive and capacitive. In previous studies, the resistive type was widely used because of the simplicity of its fabrication process, its ability to apply a newly designed sensitive film to the measurement section, and its superior detection speed.[9–11] Evaluation studies reported good detection speed at room temperature. However, challenges exist for detection under low-humidity conditions of approximately 10% relative humidity (RH) and across a range of temperatures. The capacitive type shows higher linearity, accuracy, and thermal stability than the resistive type. The capacitive type has two main structural types: comb and parallel plate. Comb-type capacitors also require fewer processes to manufacture, and previous studies have indicated that they exhibit good response in the low humidity range, which was an issue with the resistive type.[12,13] However, sensor size presented challenges. The parallel-plate capacitor requires electrodes on top of the sensing film, which complicates the fabrication process and imposes process restrictions on the sensing film material. The parallel-plate capacitor also has the benefit of higher detection sensitivity than the comb-type capacitor and shows excellent performance even in a small area.[14] However, whether the stability of sensors small enough to be mounted in 1 mm^2 packages is sufficient remains unclear. In addition, previous studies did not examine the stable operation of sensors after the actual packaging process.

In this study, we fabricated and evaluated a humidity microsensor with a parallel-plate capacitor that can be mounted in a microhermetic package and can stably measure humidity, even with a simple detection system. To miniaturize the sensor, we used polyimide, which has an affinity for the MEMS process and changes its relative permittivity as it absorbs moisture. Additionally, we assessed whether the sensor could detect the environment inside the package by mounting it inside a microhermetic package. The RH in the package only increases over time under accelerated test conditions in the case of package leakage. Therefore, a sensor accuracy of ±5% is sufficient for evaluation. As the package size is <1 mm^2, the target size of the humidity sensor is also <1 mm^2. In a previous study, we measured long-term reliability as a change in capacitance using wireless measurement with a coupling coil.[15] However, this method requires placing the coil inside the package, leading to an unnecessary increase in package size. Therefore, we employed the method of removing the hermetic conductor from the package and directly probing the conductor.

2. Data, Materials, and Methods

2.1 Fabrication of humidity microsensor

Figure 2(a) illustrates the process flow for fabricating the humidity microsensor in this study. The fabrication process involved photolithographic patterning on borosilicate glass (D 263® T eco, Schott). A 50 nm Ti layer and a 200 nm Au layer were deposited on the glass via RF sputtering to form the first layer. The second layer was a 200 nm insulating film of polyimide (PYRE-ML, I.S.T.), which was deposited by diluting it three times with 99% 1-methyl-2-pyrrolidone (NMP, Wako). Oxygen plasma treatment (O_2: 15 sccm, 25 W, 1 s) using an etching system (FA-1, Samco) was performed to promote adhesion between the polyimide and metal

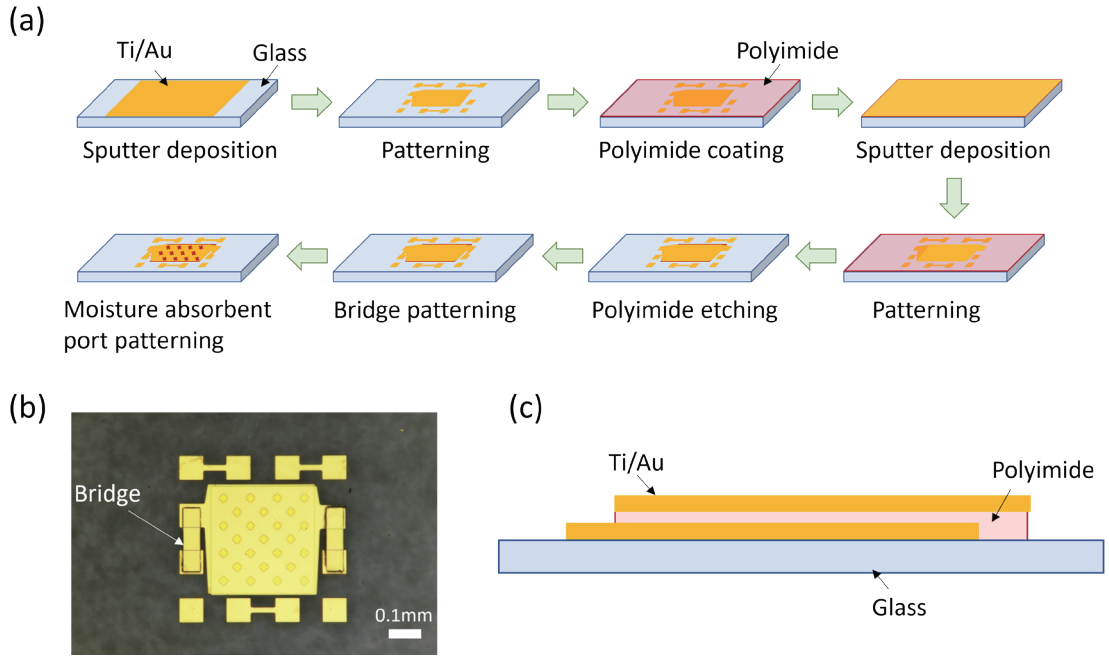

Fig. 2. (Color online) (a) Schematic of humidity microsensor fabrication process. (b) Top view and (c) cross-sectional schematic of humidity microsensor.

layers. A 50 nm Ti layer and a 200 nm Au layer were then deposited on the glass via RF sputtering to form the third layer. The patterned third layer was used as a mask to remove excess polyimide by dry etching (O_2: 20 sccm, CF_4: 3 sccm, 1 min). The patterning exposure system used in this study was a maskless exposure system (PALET, NEOARK). The etchant used for electrode patterning was 0.21 mol/l iodine solution (Au) and Pure Etch TE-307 (Hayashi Pure Chemical) (Ti). As the metal layer on the top surface is formed on polyimide, it is weak and can lead to mounting failure under load. To address this, a bridge structure was used to connect the topmost metal layer and the bottom metal layer to ensure stable mounting. Patterns for humidity absorption were then formed. The size was <0.5 mm^2, including the sensing area and mounting pad. Figures 2(b) and 2(c) illustrate the top view and cross-sectional schematic of the fabricated humidity microsensor, respectively. The sensors were separated using a femtosecond laser oscillator (μJEWEL D-1000, IMRA) on a laser processing machine (LWL-3030, SIGMA KOKI).

2.2 Humidity response test conditions

In the humidity response test, the humidity microsensor was mounted on an evaluation substrate, which was placed on a patterning glass with a metal layer deposited by sputtering a 50 nm Ti layer and a 200 nm Au layer [Fig. 3(a)]. The humidity microsensor was then die-bonded with epoxy resin (OD2002, Epotek) and wire-bonded using a multibonder (7700D, HISOL).

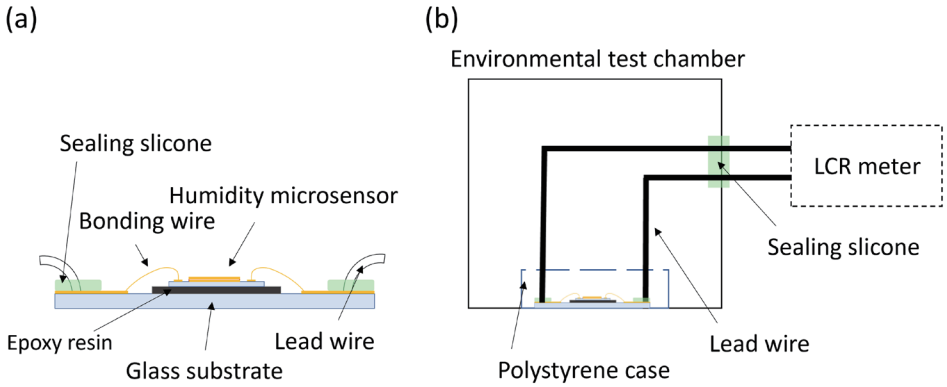

Fig. 3. (Color online) (a) Schematic of sample for humidity response evaluation. (b) Schematic of humidity response test conditions.

Lead wires were bonded using solder, and the bonding area was protected with silicone (MED-4211, Nusil). The response of the humidity microsensor was evaluated using a small environmental test chamber (SH220, ESPEC) in the RH range of 10–85 at 35% RH, the lowest value that can be set at 70 °C. Capacitance was measured under each RH condition, where RH was kept constant for 3 h and then changed by 10% over 1 h. At 25 °C, measurements were taken in 10% increments up to 90% based on the lower limit of 50%. Capacitance measurements were taken at 100 kHz, 0.1 V, and 100 s intervals using an LCR meter (ZM2371, NF). Hysteresis measurements were evaluated by averaging the capacitance values measured during discontinuous moisture absorption and desorption. Figure 3(b) illustrates the test setup used to measure the humidity response. To protect the humidity microsensor, measurement samples were placed in a porous polystyrene case. The inside and outside of the chamber were separated by a silicone stopper, and the lead wires were connected to the LCR meter through the inside of the silicone. To remove any effect from the substrate and lead wires on the measurement results, the measurement results were calibrated by comparing the results obtained when the sensor was mounted with those obtained when the sensor was not mounted on the substrate.

2.3 Fabrication of microhermetic package

The mounting substrate used in this study was a custom-made glass substrate with vertically embedded conductors (Ti) manufactured by TECNISCO, LTD. The humidity microsensor was die-bonded with epoxy resin (OD2002, Epotek) and wire-bonded with a multibonder (7700D, HISOL). Figure 4 illustrates the process flow for fabricating the microhermetic package used in this study. A 0.5-mm-thick glass lid with a 0.3 mm cavity structure made of borosilicate glass (D 263® T eco, Schott) and metal sputtering (Ti-50 nm/Pt-50 nm/Au-200 nm) was thermally pressed onto a silicon substrate patterned with gold submicron particles to transfer the pattern. A glass lid with transferred patterns was bonded to the sensor-mounted through-glass via substrate.[16] The bonding process was performed at 200 °C in an inert gas environment after drawing to a high vacuum. The packaging process was performed by MEMSCORE Co., Ltd.

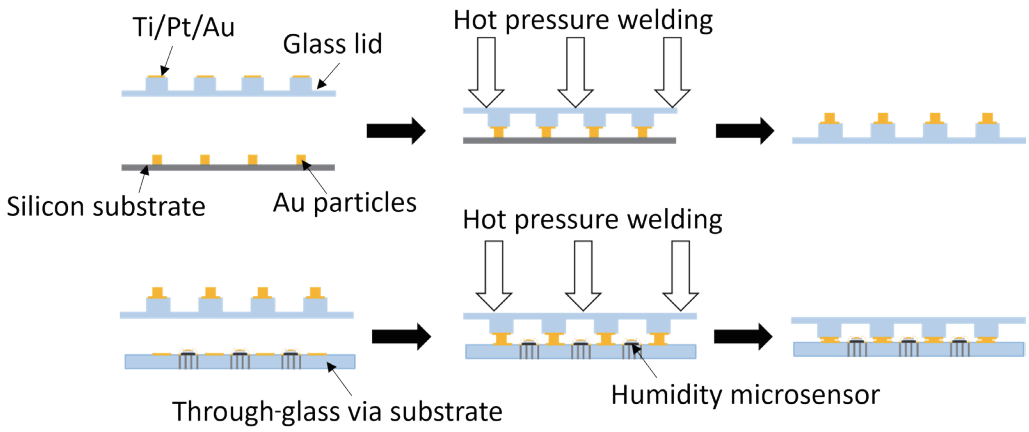

Fig. 4. (Color online) Schematic of fabrication process for microhermetic package.

2.4 Accelerated life testing

To mimic an environment of extracellular tissues, the samples were immersed in 0.01 mol/L phosphate-buffered saline (PBS) (with a pH range of 7.2–7.4) at a temperature of 87 °C. The samples were then measured by removing them from the PBS and probing them into a through-glass via. The acceleration factor was calculated using the Arrhenius equation with Eq. (1),[17] where the experimental temperature T was set to 87 °C and the body temperature T_{nat} was 37 °C. The resulting acceleration factor was 32.

$$\begin{aligned} &Accelarated\ aging\ by\ factor = f \\ &f = 2^{\Delta T/10} \\ &\Delta T = T - T_{nat} \end{aligned} \tag{1}$$

It is recommended that the hermeticity of the implant device be 5000 ppm (below 6000 ppm), which is the allowable water vapor partial pressure for condensation to occur at 0 °C.[18] A water vapor partial pressure of 5000 ppm corresponds to a RH of approximately 16% at 25 °C and 1 atm. Therefore, the accelerated life testing was set to end at a 16% increase in RH. The RH in the package was calculated by creating a linear approximation equation from the value obtained during the humidity response test. The water leak rate can be obtained using Eq. (2).[19]

$$L_{H_2O} = -\frac{V}{t}\left[\ln\left(1 - \frac{Q_{H_2O}}{\Delta pi_{H_2O}}\right)\right], \tag{2}$$

where L_{H_2O} is the true water leak rate, Q_{H_2O} the amount of water that has leaked in, V is the internal volume of the package in cc, t is the time in seconds (in case, the time is determined by the multiplication of the accelerated life testing time and the acceleration factor of 32), and

Δpi_{H_2O} is the initial difference in the water partial pressure of the outside less the partial pressure on the inside of the package (in this case, 0.003).

Assuming the temperature and atmosphere at the time of microhermetic package fabrication, the RH in the package before the accelerated life testing was assumed to be 0%. The saturated water vapor pressure in the package at this time can be expressed using Eq. (3) on the basis of the Tetens equation.[20]

$$e(T) = 6.1078 \times 10^{(7.5 \times T/(T+237.3))}, \tag{3}$$

where $e(T)$ is the saturation vapor pressure and T is the temperature.

The relationship between the volumetric humidity VH and the relative humidity RH is expressed as,

$$VH = \frac{217 \times e(T)}{T + 273.15} \times \frac{RH}{100}. \tag{4}$$

Therefore, Q_{H_2O} that has entered the package is the VH multiplied by the volume of the package.

3. Results and Discussion

3.1 Evaluation of humidity microsensor

To assess the characteristics of the humidity microsensor, we measured the capacitance of the sensor as the RH around it changed using a small environmental testing machine. Figures 5(a) and 5(b) illustrate typical examples of the measurement results. The findings indicate that the capacitance of the humidity microsensor varies with the RH in the environmental test chamber. To clarify the hysteresis, we compared changes in the capacitance of the humidity microsensor at 70 °C with moisture absorption and desorption [Fig. 5(c)]. These results showed no significant hysteresis. Moreover, the maximum hysteresis was 1.32 at 65% RH. To determine whether the sensor characteristics vary with the operating temperature, we evaluated the capacitance at various relative humidities at 70 and 25 °C [Fig. 5(d)]. The maximum hysteresis was calculated to be only 1.32%, using the change in capacitance with increasing humidity. A regression line of capacitance values at each RH showed that $C_{(RH)}$ (pF) = 0.064 (RH) + 13.988 at 70 °C (RH 35–85%) and $C_{(RH)}$ (pF) = 0.059 (RH) + 14.289 at 25 °C (RH 50–90%). During these measurements, we observed no significant changes in sensor characteristics at the operating temperature. The measurement accuracies were ±4.52% at 70 °C and ±1.88% at 25 °C. Moreover, the humidity response accuracy was lower at 70 °C than at 25 °C. We consider the reduction in accuracy in the high humidity range of 70 °C to be due to polyimide-derived characteristics. These results suggest that the amount of RH change in the environment can be measured by monitoring the changes in the capacitance value of the fabricated humidity microsensor.

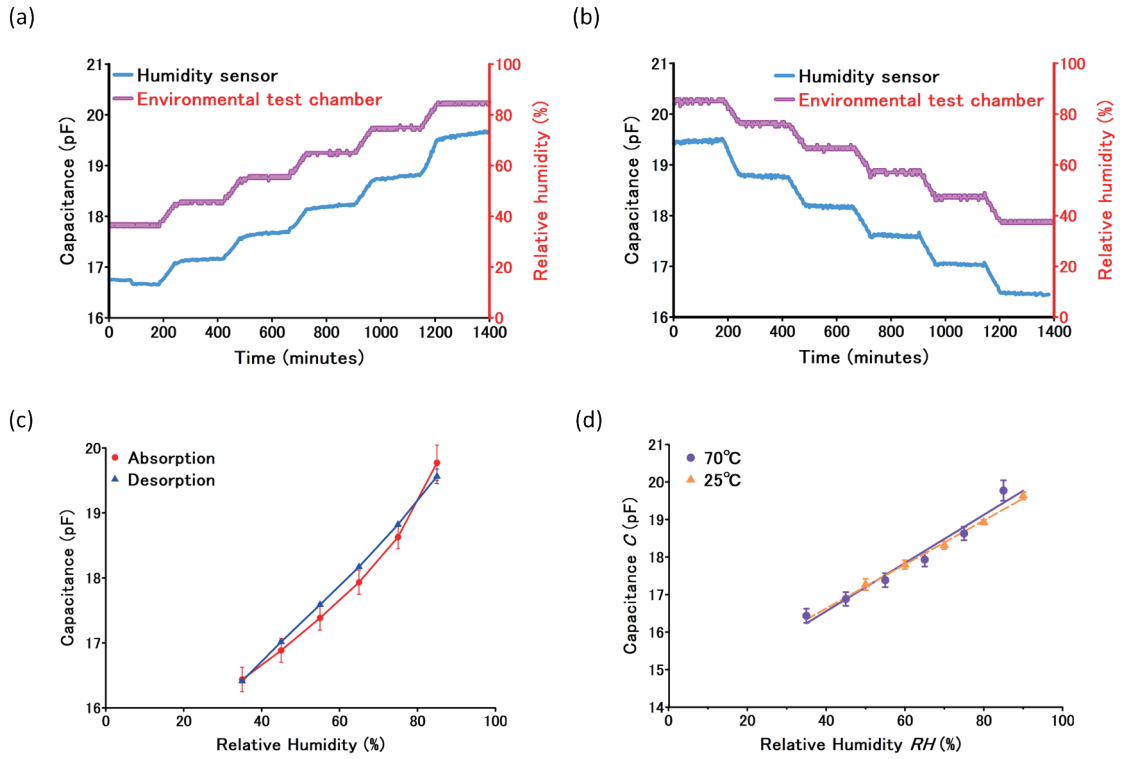

Fig. 5. (Color online) (a) Typical example of capacitance change with increasing RH at 70 °C. (b) Typical example of capacitance change with decreasing RH at 70 °C. (c) Hysteresis curve under 70 °C conditions. Moisture absorption and desorption represent averages of discontinuous measurement ($N = 3$). Error bars reflect the ± standard error of the mean (S.E.M.). (d) Average capacitance at each RH ($N = 3$). The solid line is a regression line at 70 °C (coefficient of determination $r^2 = 0.967$). The dotted line is a regression line at 25 °C (coefficient of determination $r^2 = 0.995$). Error bars are ± S.E.M.

3.2 Evaluation of microhermetic packages with humidity microsensors

Long-term reliability evaluations typically involve accelerated life testing, which exposes the device to temperatures higher than expected for its operating temperature. As a result, evaluation sensors must be able to withstand the test temperatures as well as the packaging process. To verify the sensor's ability to measure correctly under these conditions, we mounted it in a micropackage and conducted tests (Fig. 6). The package is 1.2 by 1.2 mm and 0.75 mm high, and has an internal volume of 2.165×10^{-4} cm^3 [Figs. 6(a) and 6(b)]. For a temperature of 25 °C, the endpoint of the accelerated life testing was set at a 16% increase in RH (refer to the Methods section). The approximate equation obtained in Fig. 5(d) includes the capacitance components of the glass substrate and lead wires. However, the humidity microsensor part is the dominant contributor to the total capacitance change. Moreover, the capacitance of the through-glass via substrate remained stable at approximately 0.4 pF during the accelerated life testing (data not shown). Thus, on the basis of the slope of the approximate equation, an increase of 0.944 pF at 25 °C was set as the endpoint for the amount of change in RH. The results of the accelerated life testing revealed that all samples exceeded the endpoint on the 5th day of the test. Sample No. 5,

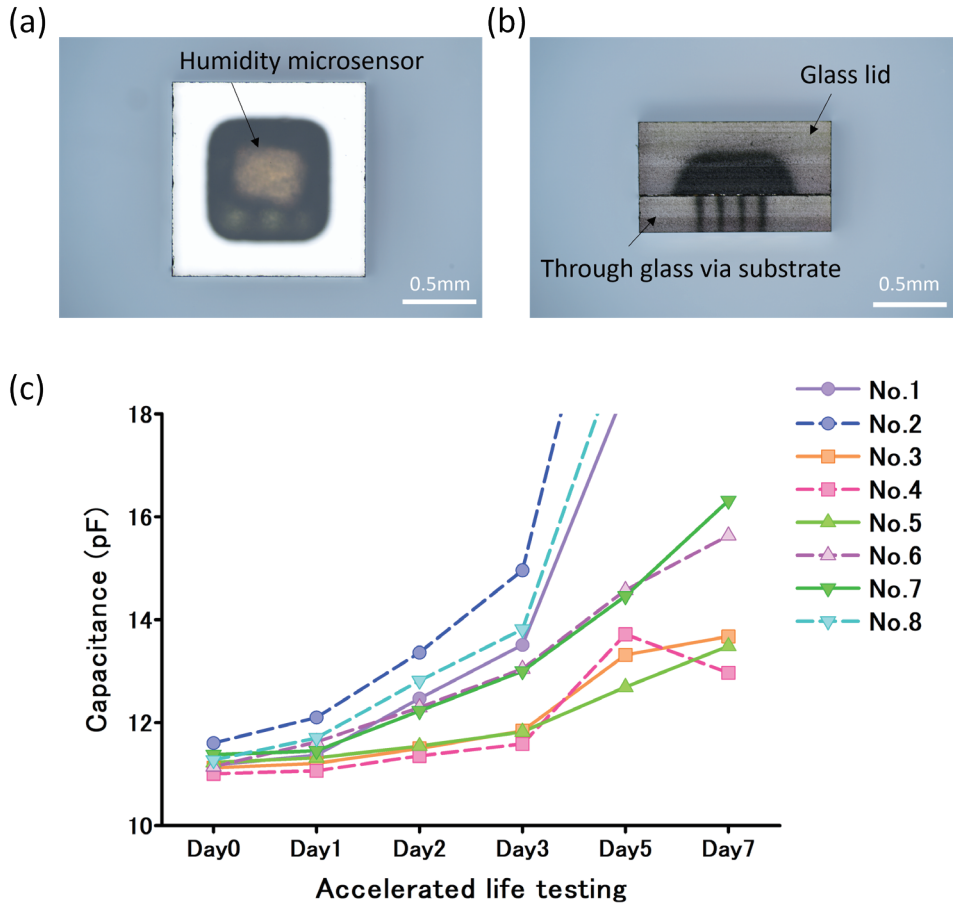

Fig. 6. (Color online) (a) Top and (b) side views of a small hermetic package. (c) Evaluation of capacitance values during accelerated life testing.

which had the lowest capacitance on the 5th day of the accelerated life testing, was used as a typical example. Furthermore, the inside of the micropackage was filled with inert gas. Therefore, RH was 0% at the start of the test. From the slope of the approximate equation, the RH on the 5th day of the accelerated life testing was 24.8%. Under these conditions, the water leakage rate was 6.469×10^{-18} atm-cm^3/s (refer to the Methods section). This leakage rate exceeds the general He leakage test limit, which can detect fine leaks.[3,21] These findings suggest that the fabricated humidity microsensor is capable of withstanding the test temperature and the micropackaging process, and that it is possible to evaluate micropackage performance.

3.3 Sensor validity assessment

The results suggest that the fabricated sensor is effective for micropackage evaluation. However, it is also possible that the capacitance increase is due to factors other than leakage. Therefore, we exposed the fabricated sensor to the same 87 °C environment used in the accelerated life testing and verified if there were any changes in their response to environmental

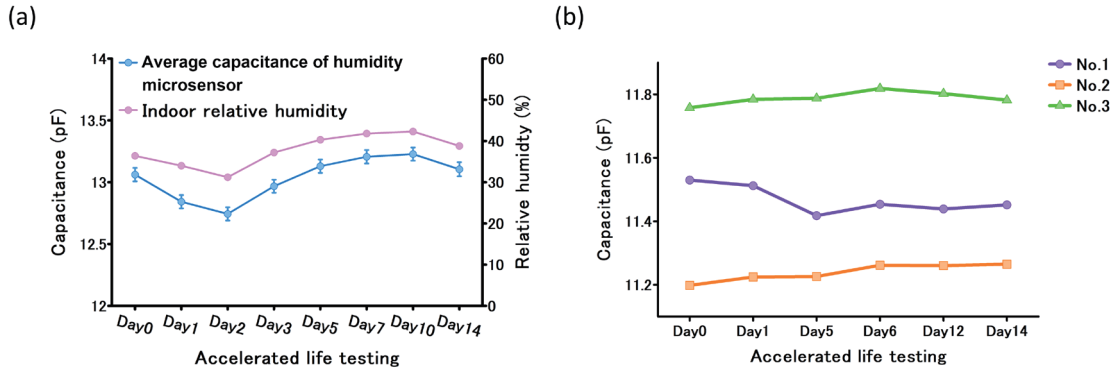

Fig. 7. (Color online) (a) The upper line is the RH in the room during the testing period. The bottom line is the average capacitance change under the accelerated life testing conditions without PBS (N = 12). Error bars are ± S.E.M. (b) Capacitance change in a small hermetic package under accelerated life testing conditions without PBS.

Table 1
Summary of performance and requirements for humidity microsensor and micropackage.

	Requirements	Performance
Sensor size	<1 mm^2	<0.25 mm^2
Humidity microsensor accuracy	±5%	±4.52% (70°C); ±1.88% (25°C)
Micropackage stability	Over 5 years (37°C)	5 days (87°C); 160 days (37°C)

humidity. As a result, the capacitance changed according to the RH in the environment during the 14 days of testing [Fig. 7(a)]. The results indicate that the increase in the capacitance of the sensor mounted in the package is not reproducible only by applying the same thermal cycle. We exposed the microhermetic packages to an 87 °C environment without PBS from the accelerated test to investigate whether capacitance change was caused by outgassing induced in the package. The results demonstrated that the capacitance in the package remained stable during the accelerated life testing period [Fig. 7(b)]. Therefore, the results suggest that the fabricated sensor senses changes in capacitance due to moisture entering from the external environment. Table 1 shows a summary of the performance characteristics of the fabricated humidity microsensor and the evaluated micro package.

4. Conclusions

Our study demonstrated that a humidity microsensor, fabricated through simple photolithography, can facilitate monitoring the environment inside a microhermetic package. Conventional package performance evaluation methods require expensive measurement systems that depend on package size. However, our humidity microsensor is superior owing to its ability to directly measure the RH inside a package using a simple measurement system. Additionally, the polyimide material used in our micor sensor is stable over a wide range of temperatures and resistant to heat treatment during encapsulation. Therefore, our microsensor can be used to

evaluate packages manufactured under various encapsulation conditions. Our microsensor also enables the reliability evaluation of devices other than retinal prostheses that require miniaturization. However, we could not measure capacitance below 35% RH in this study owing to the limited humidity range of the environmental test chamber. Thus, actual measurements in low-humidity regions are necessary to obtain more accurate RH values inside the package. Despite this limitation, the hermetic package performance required for hermetically sealed devices demands that the RH inside the package remains constant over the expected period of use. Therefore, the humidity microsensor developed in this study is sufficient for package evaluation. In the future, we aim to develop a microthermal package with long-term durability for retinal prosthesis using the fabricated microsensor and measurement system.

Conflicts of interest

Takuro Kono and Yasuo Terasawa are employees of Nidek Co., Ltd. Hiroyuki Tashiro and Jun Ohta received a research grant from Nidek Co., Ltd.

References

1 T. Fujikado, M. Kamei, H. Sakaguchi, H. Kanda, T. Endo, M. Hirota, T. Morimoto, K. Nishida, H. Kishima, Y. Terasawa, K. Oosawa, M. Ozawa, and K. Nishida: Investig. Ophthalmol. Vis. Sci. **57** (2016) 6147. https://doi.org/10.1167/iovs.16-20367
2 Y. Nakanishi, K. Sasagawa, R. Siwadamrongpong, K. Shodo, Y. Terasawa, H. Takehara, M. Haruta, H. Tashiro, and J. Ohta: J. Appl. Phys. **62** (2023) SC1077. https://doi.org/10.35848/1347-4065/acb77d
3 Investigational Device Exemption (IDE) Guidance for Retinal Prostheses: https://www.fda.gov/regulatory-information/search-fda-guidance-documents/investigational-device-exemption-ide-guidance-retinal-prostheses (accessed March 2023).
4 MIL-STD-883K, 1014.15.
5 K. Kawasaki and K. Senzaki: Jpn. J. Appl. Phys. **1** (1962) 223. https://doi.org/10.1143/JJAP.1.223
6 K. H. Yoon, H. Kim, Y.-E. Koo Lee, N. K. Shrestha, and M. M. Sung: RSC Adv. **7** (2017) 5601. https://doi.org/10.1039/C6RA27759D
7 C. Li, M. Cauwe, L. Mader, D. Schaubroeck, and M. Op de Beeck: Coatings **10** (2019) 19. https://doi.org/10.3390/coatings10010019
8 T. J. Harpster, S. Hauvespre, and M. R. Dokmeci: J. Microelectromech. Syst. **11** (2002) 1. https://doi.org/10.1109/84.982864
9 G. Dubourg, A. Segkos, J. Katona, M. Radović, S. Savić, G. Niarchos, C. Tsamis, and V. Crnojević-Bengin: Sensors **17** (2017) 1854. https://doi.org/10.3390/s17081854
10 L. Liu, X. Ye, K. Wu, R Han, Z. Zhou, and T. Cui: Sensors **9** (2009) 1714. https://doi.org/10.3390/s90301714
11 V. S. Turkani, D. Maddipatla, B. B. Narakathu, T. S. Saeed, S. O. Obare, B. J. Bazuin, and M. Z. Atashbar: Nanoscale Adv. **1** (2019) 2311. https://doi.org/10.1039/C9NA00179D
12 L. Gu, Q. A. Huang, and M. Qin: Sens. Actuators, B **99** (2004) 491. https://doi.org/10.1016/j.snb.2003.12.060
13 S. Ali, M. A. Jameel, A. Gupta, S. J. Langford, and M. Shafiei: Synth. Met. **275** (2021) 116739. https://doi.org/10.1016/j.synthmet.2021.116739
14 M. Dokmeci and K. Najafi: J Microelectromech. Syst. **10** (2001) 2. https://doi.org/10.1109/84.925735
15 T. Kono, Y. Terasawa, H. Tashiro, T. Ueno, and J. Ohta: Sens. Mater. **34** (2022) 4. https://doi.org/10.18494/SAM3727
16 H. Ishida, T. Ogashiwa, T. Yazaki, T. Ikoma, H. Kusamori, and J. Mizuno: Trans. Jpn. Inst. Electron. Packag. **3** (2010) 1. https://doi.org/10.5104/jiepeng.3.62
17 General Aging Theory and Simplified Protocol for Accelerated Aging of Medical Devices: https://www.mddionline.com/design-engineering/general-aging-theory-and-simplified-protocol-accelerated-aging-medical-devices?_sp=70e6e4f1-0455-4490-b637-560a70b71e66.1645495498350 (accessed March 2023).

18 G. Jiang and D. D. Zhou: Implantable Neural Prostheses 2, D. D. Zhou and E. Greenbaum, Eds. (Springer Science + Business Media, LLC, New York, 2010) Chap. 2. https://doi.org/10.1007/978-0-387-98120-8_2
19 H. Greenhouse, R. Lowry, and B. Romenesko: Hermeticity of Electronic Packages (Elsevier, Oxford, 2012), 2nd ed., Chap. 9.
20 O. Tetens: Z. Geophys. **6** (1930) 297.
21 MIL-STD-750E, 1071.8.